MINERALOGICAL MAGAZINE, SEPTEMBER 1986, VOL. 50, PP. 491–502

Complex sequential pyroxene growth in tholeiitic hypabyssal rocks from southern West Greenland

R. P. HALL AND D. J. HUGHES

Department of Geology, Portsmouth Polytechnic, Burnaby Road, Portsmouth, PO1 3QL

AND

C. R. L. FRIEND

Department of Geology and Physical Sciences, Oxford Polytechnic, Headington, Oxford OX3 0BP

ABSTRACT. Chemically complex pyroxenes which occur in early Proterozoic tholeiitic dolerite dykes in southern West Greenland have been investigated using back-scattered electron (BSE) imagery, X-ray mapping and electron microprobe analysis. A wide variety of compositions occur within individual pyroxene grains in these rocks. They can be explained by simultaneous nucleation of different pyroxenes, the evolution of domains around these nucleii as a response to differential chemical gradients and the sequential precipitation of different pyroxenes at progressively lower temperatures. As an example, the individual grains in one dyke sample contain domains of bronzite, hypersthene, magnesium pigeonite, augite, and subcalcic augite. Olivine in this sample varies in composition from Fo_{70} to Fo_{33}, although individual grains are only weakly zoned. The wide variation in pyroxene and olivine compositions suggests ranges of crystallization temperatures from *c.*1250° to as low as 825 °C. Such compositionally variable pyroxenes are possibly characteristic of hypabyssal tholeiitic rocks.

KEYWORDS: pyroxenes, hypabyssal, back-scattered electron imagery, West Greenland.

TWO principal oversaturated basic igneous pyroxene assemblages occur in nature. The first comprises magmatically equilibrated pyroxenes, the compositions of which reflect the chemistry of the liquids from which they precipitate. Equilibrated pyroxene evolution trends are defined by the mineralogy of progressively evolved magma bodies, as for example in large layered intrusions or in simple basaltic low-pressure fractional crystallization systems. Classic examples of this are the tholeiitic pyroxene evolution trends of the Skaergaard layered intrusion (Wager and Brown, 1968) and the Thingmuli volcano (Carmichael, 1967). In contrast to these are the compositionally variable, quenched, metastable, groundmass pyroxenes which typify many lavas (e.g. Ewart, 1976; Arndt and Fleet, 1979). The present study demonstrates the presence of a distinctive third type of pyroxene assemblage, found in hypabyssal rocks, with characteristics intermediate to those of fully equilibrated and quenched pyroxenes.

The MD dykes

An extensive suite of samples has been examined from a major swarm of large basic dykes which occurs within the Archaean craton of southern West Greenland (Hall *et al.*, 1985). This dyke swarm was first recognized in the Ketilidian (Proterozoic) belt to the south of the Archaean craton (Allaart, 1976) and became known as the 'MD' (metadolerite) dyke swarm since the dykes are metamorphosed and deformed in this region. However, throughout the Archaean terrain they are neither metamorphosed nor deformed. Most have completely fresh primary mineral assemblages although some have suffered deuteric alteration and shearing, presumably as a consequence of their emplacement along active shear zones (Chadwick, 1969). The dykes are nearly all vertical, and three principal generations (MD1, MD2, and MD3) have been distinguished by their cross-cutting relationships. Rb/Sr isotope analysis by Kalsbeek and Taylor (1985) has yielded an emplacement age of 2133 ± 63 Ma.

Geochemically, the swarm has a general tholeiitic trend (fig. 1) with the oldest dykes being the most magnesian and the youngest ones the most Fe-rich (Mg/(Mg + Fe) ionic ratios of *c.*0.8 and 0.35 respectively) (Rivalenti, 1975; Hall *et al.*, 1985). The differences in geochemistry between the three major dyke generations are reflected by variations in mineral chemistry. The most magnesian rocks contain the most magnesian pyroxenes while the

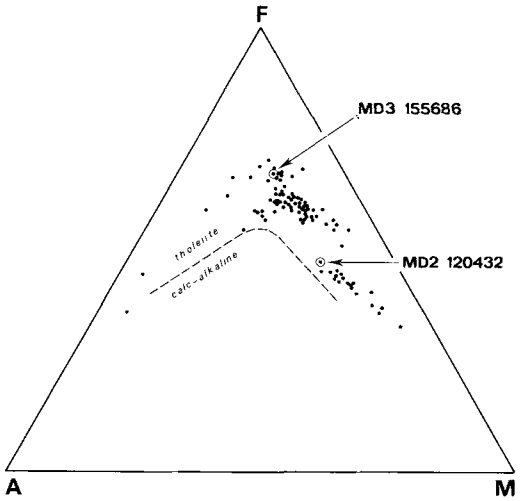

FIG. 1. Compositions of the MD dykes in terms of $A(Na_2O+K_2O):F(FeO+Fe_2O_3):M(MgO)$, defining a typical tholeiitic Fe-enrichment trend (after Rivalenti, 1975; Hall *et al.*, 1985). The line separating the calc-alkaline and tholeiitic fields is taken from Irvine and Baragar (1971).

more Fe-rich dykes carry correspondingly Fe-rich pyroxenes. However, an extensive electron microprobe study of the pyroxenes in these dykes has shown that the pyroxene variation within any one sample is often greater than the variation from one dyke to another or from one generation of dykes to another. Four or five different pyroxene phases are commonly present not merely in individual rock samples but, in some instances, in individual grains.

The most complex pyroxene grains within the MD dykes occur in some of the second and third generation (MD2 and MD3) dolerites. The complexity of these grains has been crudely demonstrated by intensive microprobe analysis and the contouring of the microprobe data on grain maps (Hall *et al.*, 1985). However, high-resolution backscattered electron (BSE) imagery has now revealed the intricate compositional detail of these pyroxenes. Some of the results of this work are presented here.

Analytical techniques

Geochemical data (major and trace elements) were determined by X-ray fluorescence analysis using a Philips PW 1410 semi-automatic spectrometer at the Department of Geology, Portsmouth Polytechnic, using the conditions and data retrieval techniques described by Brown *et al.* (1973). FeO was determined by titration using the method of Wilson (1955). Rare-earth element (*REE*) data were determined by neutron activation analysis at the Manchester and Liverpool Universities Reactor Centre, Risley. Microprobe analyses were carried out by us using the energy dispersive facilities at the Department of Earth Sciences, Cambridge University, and the wavelength dispersive instrument at the Department of Earth Sciences, Oxford University. A brief summary of operating conditions was presented by Hall *et al.* (1985). BSE images and Mg, Fe, and Ca X-ray maps of minerals were made by us using the JEOL 35 and JEOL 840 scanning electron microscopes at Portsmouth Polytechnic and Oxford Polytechnic respectively. The diagrams illustrating the chemical complexity of the pyroxene grains are based on combined BSE, X-ray map and electron microprobe data.

MD2 dyke GGU 120432

Pyroxenes. Of the sixteen MD dykes which have so far been investigated in detail, the one which contains the widest spectrum of pyroxene compositions within individual complex grains is one of the second generation (MD2) dolerites. The sample (GGU 120432) was taken from the core of a typical 20 m wide, 030°-trending, vertical MD2 dyke from the southern Fiskenaesset region (fig. 2). It comprises an apparently normal, medium-grained (*c.*2 mm), sub-ophitic olivine-bearing dolerite (fig. 3). Chemically, the rock falls approximately one-third of the way along the overall evolution trend of the MD dyke swarm (fig. 1, Table I). It has an ionic Mg/(Mg+Fe) value of 0.6 and a slightly evolved *REE* distribution pattern ($La_N/Lu_N = 3.2$) with light and heavy *REE* values respectively about 29 and 9 times those of average CI chondrite (chondrite data from Evensen *et al.*, 1978).

Despite the unremarkable texture and geochemistry of this dyke (Table I), it has an exceptionally large compositional range of pyroxenes which

TABLE I. Geochemical analyses of a) GGU 120432 and b) GGU 155686.

wt%*	(a)	(b)	ppm	(a)	(b)	ppm	(a)	(b)
SiO_2	50.45	48.19	Sc	20	27	La	7.2	24.9
Al_2O_3	16.95	15.73	V	184	360	Ce	16.0	57.0
Fe_2O_3	0.77	3.98	Cr	152	18	Pr	2.3	7.6
FeO	8.69	11.35	Ni	132	49	Nd	10.6	33.0
MgO	7.65	4.73	Cu	52	293	Sm	2.3	7.3
CaO	11.39	10.02	Zn	70	112	Eu	0.99	2.35
Na_2O	2.42	2.70	Rb	9	15	Gd	3.6	8.3
K_2O	0.58	0.76	Sr	325	268	Tb	0.38	1.15
TiO_2	0.89	2.00	Y	22	27	Dy	4.9	7.6
MnO	0.11	0.22	Zr	63	119	Er	1.6	3.6
P_2O_5	0.11	0.31	Nb	(1)	7	Yb	1.6	4.7
			Ba	186	356	Lu	0.23	0.70

*XRF major element analyses recalculated to 100% on a water-free basis.

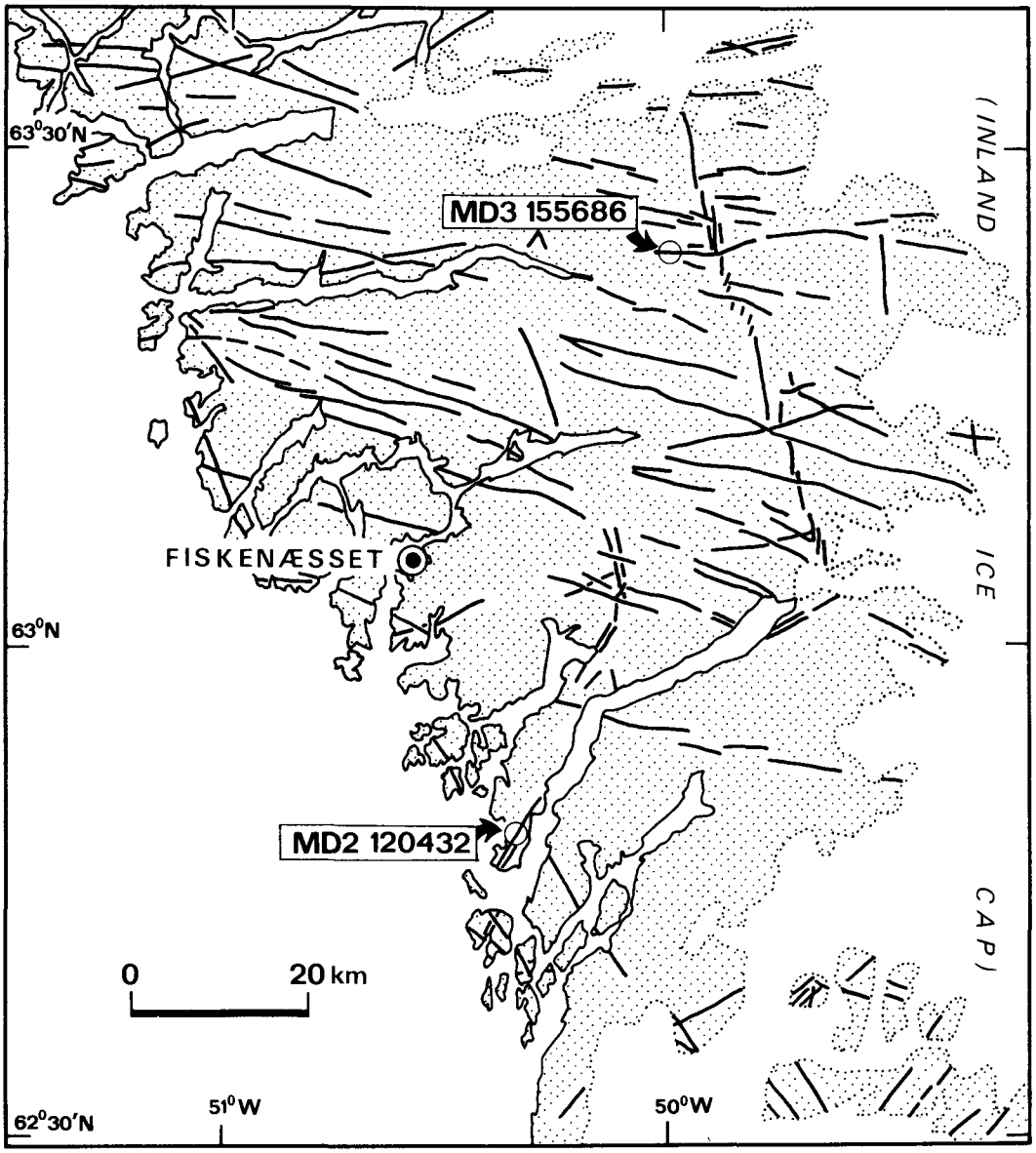

FIG. 2. Distribution of MD dykes in the Fiskenaesset region, southern West Greenland and the location of samples of MD2 dyke 120432 and MD3 dyke 155686 (after Dawes (1970), Myers (1980, 1982), Chadwick and Coe (1983) and authors' unpublished data).

comprise bronzite, hypersthene, ferrohypersthene, magnesium pigeonite, subcalcic augite, and variable augite (fig. 4). The compositions of apparently coexisting phases and erratic core to margin zoning within a few individual grains in this sample were described by Hall *et al.* (1985). The range of crystallization temperatures of the various phases can be interpreted from the temperature-contoured isobaric section through the En–Di–Hd–Fs pyroxene quadrilateral (fig. 4). The isotherms in this diagram are contoured for *c.*2.5 kbar, taken to represent the upper limit of hypabyssal pressures, and are interpolated from the 5 kbar and 1 atm data presented by Lindsley (1983). The detailed relationships between these pyroxenes revealed by BSE images and X-ray mapping have been used to

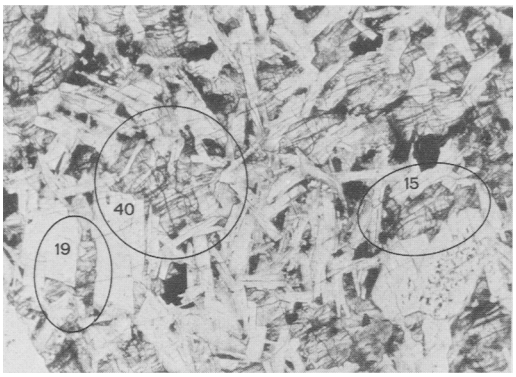

FIG. 3. Photomicrograph of MD2 dyke sample GGU 120432 showing the area of grains 15, 19, and 40 and the apparently normal sub-ophitic doleritic texture of the rock. Field of view approximately 12 × 8 mm.

determine whether or not their crystallization was simply sequential, from early-formed (*c.*1250 °C) bronzite and augite to late (1100–1000 °C) hypersthene, pigeonite, and Fe-rich, Ca-poor augite, as the graphical thermometer suggests.

Low-magnification BSE images of three typical pyroxenes in the MD2 dyke sample GGU 120432 (grains 15, 19, and 40) are presented in fig. 5. These images demonstrate that the apparently normal sub-ophitic pyroxene grains (fig. 3) comprise mosaics of compositionally variable domains. Back-scatter efficiency increases with mean atomic weight, and under the BSE conditions used for these images plagioclase appears almost black while the ore phase (exsolved titaniferous magnetite) appears white. The different compositional domains in the pyroxenes are depicted by various tonal intensities within each of the sub-ophitic grains. The darkest grey areas are bronzite and the different pale-grey tones represent subcalcic augite, Ca-poor, and Fe-rich augite, pigeonite, and hypersthene. The mid-grey areas are augite. The internal variation of these three grains and the compositions of their constituent domains are shown in fig. 6. Representative microprobe analyses of eight different compositions occurring within one grain (15) are presented in Table II.

Grain 15 in this sample (figs. 5*a*, 5*b*, 6) contains three areas of orthopyroxene, mainly zoned bronzite (*c.*En_{80}),[1] which grade into thin hypersthene margins. The calcic pyroxene component varies

[1] En values for orthopyroxene are based on X_{Mg}, where X_{Mg} = the ionic ratio Mg/(Mg+Fe).

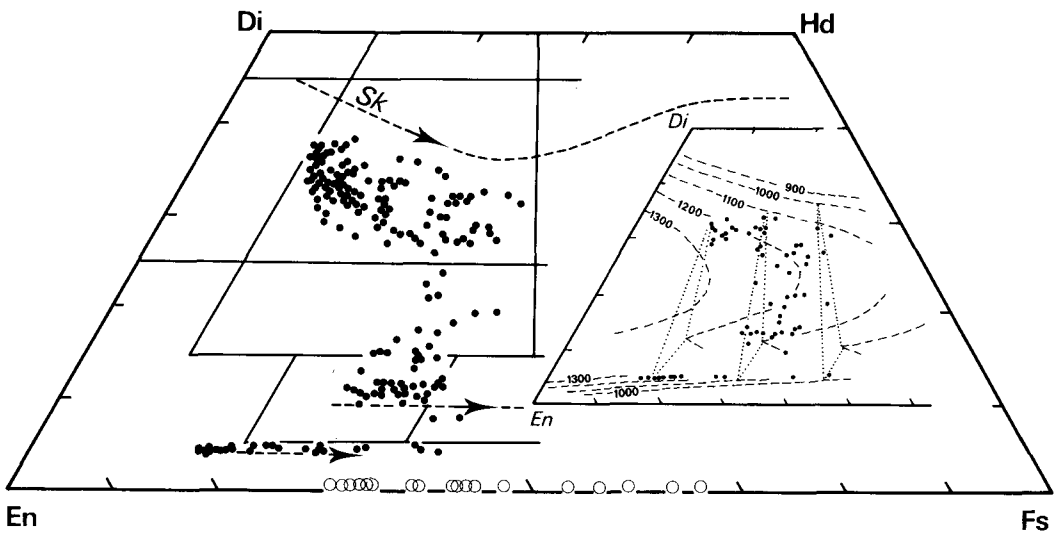

FIG. 4. Range of pyroxene compositions comprising complex grains in MD2 dyke sample GGU 120432 (excluding grains 15, 19, and 40) plotted in terms of the En($MgSiO_3$)–Di($MgCaSi_2O_6$)–Hd($FeCaSi_2O_6$)–Fs($FeSiO_3$) pyroxene quadrilateral. Olivine compositions (O) are plotted at the bottom of the diagram. The Skaergaard pyroxene evolution trend (dashed line: Sk) is drawn for comparison (Wager and Brown, 1968; Nwe, 1976). The pyroxene compositional field boundaries are taken from Poldervaart and Hess (1951). Inset diagram shows selection of pyroxene compositions recalculated to fit the graphical pyroxene thermometer according to the rules of Lindsley (1983). Isotherms drawn for a pressure of approximately 2.5 kbar. Dotted lines represent onset of three-pyroxene equilibrium assemblages at different temperatures.

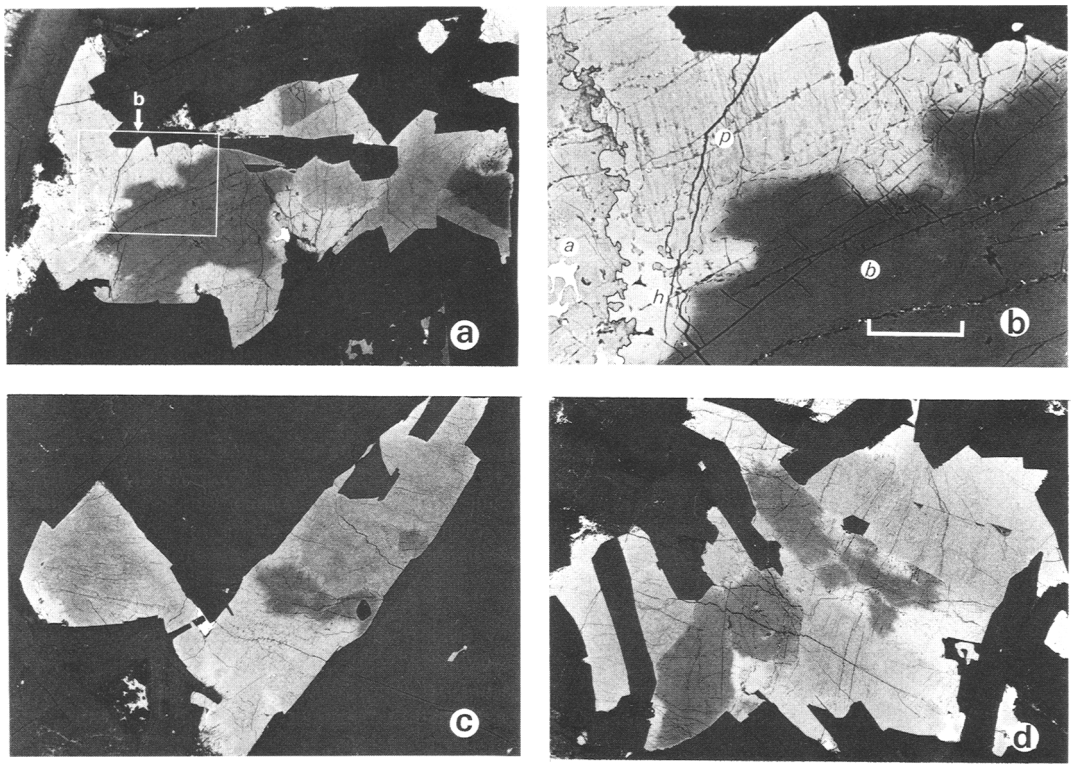

FIG. 5. BSE images of pyroxene grains 15 (*a*), 19 (*c*), and 40 (*d*) in MD2 dyke sample GGU 120432 and (*b*) the contact zone between areas of magnesium pigeonite (*p*), Fe-rich Ca-poor augite (*a*), bronzite (*b*) and (ferro-)hypersthene (*h*) at the left-hand end of grain 15. The surrounding plagioclase crystals appear almost black and Fe–Ti oxide appears white. The various shades of grey within the pyroxenes indicate the differences in composition (fig. 6). The size of the grains is indicated in fig. 6. Sharp and nebulous boundaries between the various pyroxene phases in (*b*) are enhanced by solid and dashed lines respectively. The scale bar in (*b*) represents 100 μm.

from central augite (*c*.$Wo_{38}En_{51}Fs_{11}$) to margins of slightly less calcic and more Fe-rich augite ($Wo_{33}En_{47}Fs_{20}$), which are intergrown with hypersthene (*c*.En_{60}) at the right-hand edge of the largest area of orthopyroxene in the centre of the grain. The opposite side of this orthopyroxene is intergrown with magnesium pigeonite (Wo_{7-16} $En_{50-61}Fs_{29-37}$). The central area of pigeonite shows poorly developed fine-scale blebby exsolution (fig. 5*b*) to slightly vermicular augite and hypersthene, whereas the outer edges of the pigeonite, which are in contact with neighbouring plagioclase crystals, show no evidence of exsolution. Similar magnesium pigeonite occurs in irregular patches at the upper, lower and right-hand edges of grain 15. The left-hand edge is composed of variable, Ca-poor, Fe-rich augite ($Wo_{25-33}En_{33-48}$ Fs_{25-36}). The boundary between this and the thin rim of ferrohypersthene (En_{48}), which forms the extreme left-hand margin of a large zoned bronzite, is sharp and sutured, suggesting that these two phases were competing for space during co-precipitation. The crystallization relationship between the most magnesian augite and bronzite is not so easily defined because the contacts between them are sharp and straight. Equally, the boundaries between magnesium pigeonite and Ca-poor augite are rather equivocal. None the less, the sutured contact at the left-hand end of the grain (fig. 5*b*) suggests that these two phases were precipitating simultaneously at some stage or that one was resorbing as the other was precipitating. Although hypersthene generally tends to mantle bronzite, pigeonite also occurs in large embayments in the irregular outline of the orthopyroxene domains implying that pigeonite precipitation might have superseded that of hypersthene for a period. However, the hypersthene which occurs in lamellae exsolved from the pigeonite is similar in composition (*c*.En_{60}) to that which mantles the bronzite,

TABLE II

Representative microprobe analyses of pyroxene phases in Grain 15, GGU 120432

	15/21*	15/40	15/56	15/38	15/7*	15/39	15/8*	15/60
SiO_2	54.33	52.97	50.57	52.55	51.53	53.01	50.17	50.50
TiO_2	0.18	0.53	0.28	0.52	0.43	0.27	0.48	0.49
Al_2O_3	2.50	1.23	0.99	1.21	1.67	2.61	2.51	1.59
Cr_2O_3	0.17	-	-	-	0.02	0.13	0.03	-
FeO	11.24	22.60	28.76	22.31	21.56	7.79	17.49	20.68
MnO	0.27	0.34	0.46	0.32	0.43	0.14	0.36	0.38
MgO	28.60	20.81	16.28	19.78	17.95	17.95	15.61	11.41
CaO	2.34	2.22	2.35	3.75	6.24	17.46	8.50	14.58
Na_2O	0.08	-	-	-	0.11	-	0.28	-
Total	99.82	100.69	99.68	100.43	100.13	99.35	99.31	99.63
			No. of ions on the basis of 6 oxygens					
Si	1.935	1.968	1.964	1.965	1.947	1.948	1.912	1.957
Ti	0.005	0.015	0.008	0.015	0.012	0.007	0.023	0.014
Al	0.105	0.054	0.045	0.053	0.074	0.113	0.113	0.073
Cr	0.005	-	-	-	0.004	0.004	0.001	-
Fe	0.335	0.702	0.934	0.698	0.681	0.239	0.557	0.670
Mn	0.008	0.011	0.015	0.010	0.014	0.004	0.012	0.012
Mg	1.519	1.152	0.942	1.102	1.012	0.983	0.887	0.659
Ca	0.089	0.088	0.098	0.150	0.253	0.688	0.486	0.605
Na	0.005	-	-	-	0.008	-	0.021	-
Sum	4.005	3.990	4.006	3.993	4.001	3.986	4.012	3.992
			Ionic proportions					
Ca	4.6	4.6	5.0	7.7	13.0	36.0	25.2	31.3
Mg	78.2	59.3	47.7	56.5	52.0	51.5	46.0	34.1
Fe	17.2	36.1	47.3	35.8	35.0	12.5	28.9	34.6

* Wavelength dispersive analysis; total includes traces of V, Ni and K.

suggesting that pigeonite preceded hypersthene precipitation in these cases. The lower X_{Mg} value of the ferrohypersthene (En_{48}) on the extreme left-hand side of the grain indicates that orthopyroxene precipitation either continued during that of pigeonite or subsequently resumed to outlast it.

Pyroxene grains 19 and 40 have domains with similar compositional ranges to those of grain 15 (figs. 5, 6). The longer part of grain 19 comprises areas of augite and finely exsolved pigeonite separated by a thin zone of bronzite, the length of which runs at right angles to the length of the overall grain. The augite encloses two small bronzites. Magnesium pigeonite partially envelopes the augite in the shorter limb of this grain and also occurs at the right-hand extremity of the lower limb. The distribution of the different compositional domains bears no obvious relationship to the overall shape of the grain, and appears to have resulted from either sequential crystallization or the discrete crystallization of isolated nucleii.

Grain 40 contains two large areas of bronzite around which hypersthene edges are only partially developed. Pigeonite and Ca-poor, Fe-rich augite have developed at the extremities of the grain, but pigeonite also occurs in irregular embayments in the bronzites. Similar ranges of composition and degrees of internal complexity have been mapped in numerous other grains. Some grains are dominated by orthopyroxene and others by calcic pyroxene. Some have a single large bronzite core while others contain numerous small bronzites.

Pyroxene evolution. The textural and compositional complexity of individual pyroxene grains in this MD2 dolerite do not immediately appear to conform to the simple evolution models normally attributed to the pyroxenes of tholeiitic magma suites. The main feature, albeit somewhat cryptic, which distinguishes these hypabyssal pyroxenes is the evidence for sequential growth of a variety of pyroxenes which is apparently not simple compositional zoning. This feature is not seen in equilibrated pyroxenes such as those of major plutonic intrusions and is not developed in the quenched groundmass pyroxenes of lavas. The presence of similar textures in sections taken in a variety of orientations from the rock suggests that the extent of the compositional zoning is truly three-dimensional and is not an artefact of two-dimensional sectioning.

The range of compositions occurring in the complex grains is approximately constant for pyroxenes throughout the sample (figs. 4, 6) and application of the graphical pyroxene thermometer compiled by Lindsley (1983) suggests that they crystallized over a temperature range of 1250° to about 1000 °C (fig. 4). The combined BSE and microprobe study of the pyroxene relationships in the complex grains 15, 19, and 40 demonstrates a consistent pattern of textural relationships, assum-

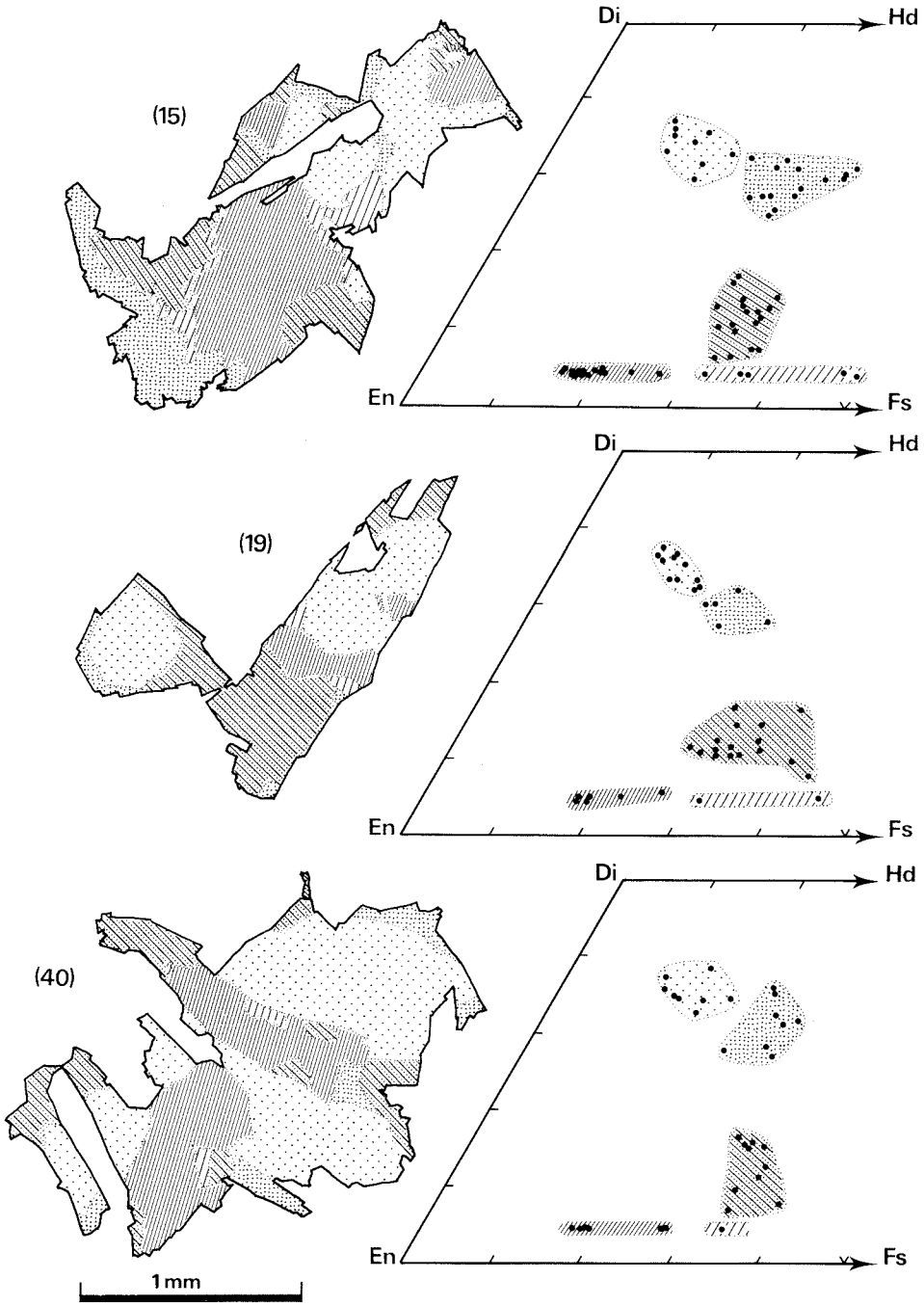

FIG. 6. Chemical morphology maps of three complex pyroxene 'grains' (15, 19, and 40) based on BSE microscopy, X-ray mapping, and electron microprobe analysis and their various compositions plotted in terms of En–Di–Hd–Fs. Shading on chemical morphology maps is equivalent to that on the corresponding pyroxene quadrilateral diagram.

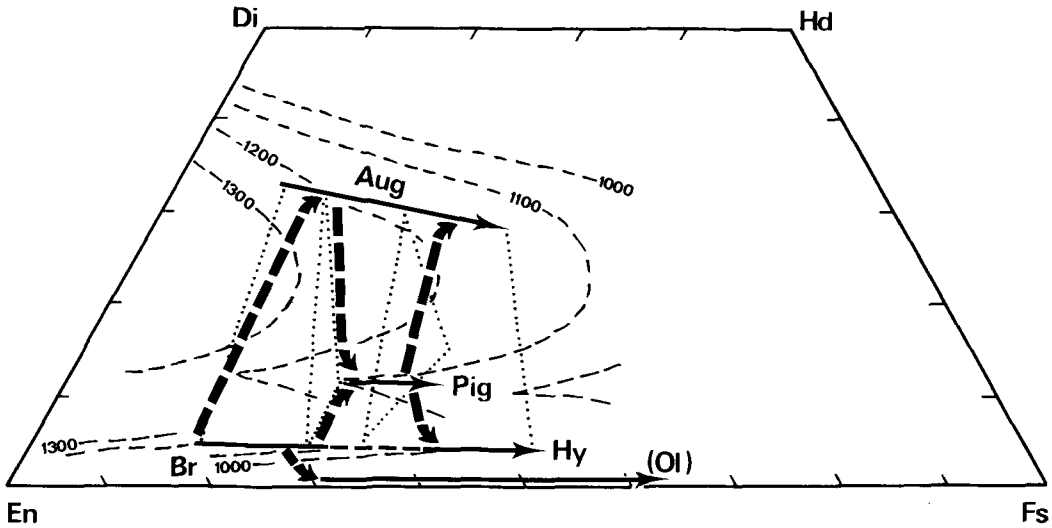

FIG. 7. Schematic summary of development of pyroxene phases within complex grains in MD2 dyke sample GGU 120432 with respect to four main genetic factors: co-precipitating phases (dotted tie-lines), chemical evolution of individual phases (solid lines), sequential precipitation of different phases (heavy dashed lines) defined by textural relationships, and variation in temperature (dashed isotherms).

ing that phases which occur at the margin of other pyroxenes are later and that phases which share complex sutured contacts were precipitated either simultaneously or after the partial resorption of one of the phases. Pyroxene phase relationships derived from the textural behaviour and the crystallization temperature estimates are summarized schematically in fig. 7.

Bronzite (En_{83}) appears to have been the first phase to precipitate (at around 1250 °C) and early bronzites are often zoned to thin hypersthene margins. Bronzite–augite relationships are mostly ambiguous, but magnesian augites (*c.*$Wo_{37}En_{52}Fs_{11}$) can occasionally be found partially enclosing bronzites and these two phases probably co-precipitated ($K_{D(Mg\text{-}Fe)^{opx\text{-}cpx}} = 1$). Magnesian augite ($X_{Mg}$ = *c.*0.8) is in turn often enclosed by hypersthene. Pigeonite precipitation succeeded that of both bronzite and augite and probably began at around 1150 °C, slightly before the crystallization of more Fe-rich augite and hypersthene. The most Fe-rich augite (*c.*$Wo_{30}En_{40}Fs_{30}$) has an equivocal relationship with pigeonite, but is probably a later, and possibly one of the final crystallizing phases, often developed at the margins of the pyroxene grains. Orthopyroxene precipitation also seems to have outlasted that of pigeonite although it is unclear whether there is a continuum of orthopyroxene compositions (En_{83}–En_{48}) or a gap in this trend in which pigeonite precipitation succeeded that of hypersthene (at X_{Mg} = *c.*0.65) to be itself superseded by Fe-rich hypersthene (X_{Mg} = *c.*0.55). The most Fe-rich augite and orthopyroxene (ferrohypersthene, *c.*En_{48}) probably crystallized simultaneously at around 1100–1000 °C.

Generally, there is good agreement between the textural and thermometric evidence for the chemical evolution of the pyroxenes, although a few relationships are somewhat contradictory. The largest area of ambiguity concerns the Ca-poor augites and pigeonites, both of which tend towards subcalcic augite compositions. In some cases Ca-poor augite crystallization seems to supersede that of pigeonite, although this is an apparently up-temperature sequence for these compositions. Pigeonite occurs most commonly both at the margins of grains and infilling hollows in the sutured outlines of early, possibly partially resorbed, high-temperature, core bronzites, while the thermometer suggests that they are a relatively low temperature precipitate (*c.*1100 °C).

Four parameters need to be evaluated in determining the evolution of these pyroxenes, namely: (i) the significance of pyroxene intergrowth textures; (ii) the recognition of pyroxene nucleation sites and determination of growth directions (for example, at the edges of complex grains) (see Dowty, 1980; Lofgren, 1980); (iii) the change in pyroxene composition implied by the solvus topology at this relatively Ca-poor part of the pyroxene composition field with respect to slight changes in *P*, *T*, and liquid composition (Mori, 1978; Huebner and

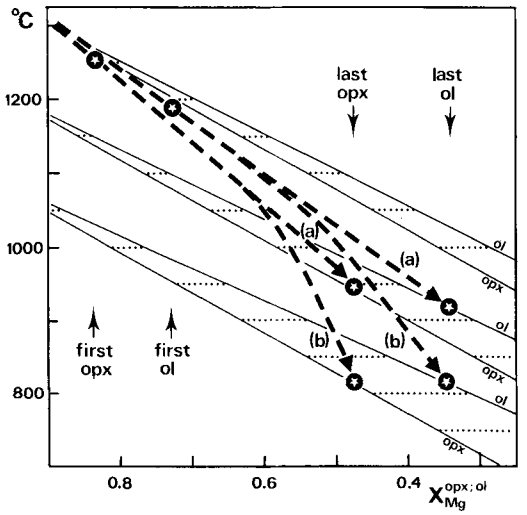

FIG. 8. Compositions of coexisting orthopyroxene (opx) and olivine (ol) (at 50° intervals, dotted lines) for three different temperature gradients (solid lines) summarized schematically from the data of Campbell and Nolan (1974) and two possible crystallization temperature gradients for GGU120432 (heavy dashed lines) inferred from the observed compositional ranges of orthopyroxene and olivine assuming either (*a*) a linear temperature gradient and orthopyroxene temperatures interpreted from the graphical thermometer of Lindsley (1983) or (*b*) that the most Fe-rich members of these phases were precipitated simultaneously.

Turnock, 1980); and (iv) the small differences in BSE tonal intensities between pigeonite, subcalcic augite and orthopyroxene where these phases have the same X_{Fe} values, although this last point can be checked by X-ray mapping and microprobe analysis.

Olivines. The crystallization interval (*c.*1250–1000 °C) suggested by the complex pyroxenes of the MD2 dyke sample (GGU 120432) is also indicated by a wide range of olivine compositions. The most magnesian olivines (Fo_{70}) are clearly the earliest and vary from subhedral to poikilitic grains, partially enclosing plagioclase and locally intergrown with or forming cores to pyroxenes. They are weakly concentrically zoned to slightly more Fe-rich margins (Fo_{60}–Fo_{50}). The most Fe-rich olivines (Fo_{33}) are late, small, interstitial grains.

This interpretation of the textural relationships of the olivines is corroborated by crystallization temperature estimates. Campbell and Nolan (1974) have investigated the influence of a_{SiO_2}, a_{FeO}, f_{O_2}, P and T on the co-precipitation of Ca-poor pyroxene and olivine. They present compositional data for orthopyroxene and olivine precipitated together at different temperatures and for different temperature gradients (at a pressure of 600 bars). Increasing the crystallization pressure expands the stability field of Ca-poor pyroxene. These data are summarized in fig. 8. Olivine which precipitated simultaneously with the most magnesian bronzite (En_{83}) in GGU 120432 would have virtually the same X_{Mg} value (*c.*Fo_{82}). However, the most magnesian olivine in this sample is Fo_{70}, which suggests that olivine precipitation followed that of bronzite (presumably at a slightly reduced a_{SiO_2}) at a temperature of around 1175 °C.

Two possible temperature gradients for GGU 120432 are also plotted on fig. 8. The first (*a*), derived from the range of orthopyroxene temperatures estimated from the pyroxene thermometer of Lindsley (1983) and the range of 'coexisting' olivine compositions, suggests that precipitation of the late-stage interstitial Fe-rich olivine (Fo_{33}) outlasted that of hypersthene (En_{48}), continuing down to a temperature of *c.*950 °C. The second (fig. 8, pathway *b*) is based on the assumption that the last interstitial hypersthene and olivine crystals were precipitated simultaneously and shows that such disparate compositions (En_{48} and Fo_{33}) could only have been co-precipitated at much lower temperatures (*c.*820 °C).

Discussion

The most characteristic and important feature of the assemblage of varied pyroxenes and olivines in the MD2 dyke (GGU 120432) is that it demonstrates (*a*) the simultaneous nucleation of different phases, (*b*) the chemical evolution (predominantly Fe-enrichment) of individual phases, (*c*) the partial resorption of early precipitated phases, and (*d*) the sequential precipitation of a variety of different pyroxenes at progressively lower temperatures. Sub-solidus re-equilibration (exsolution), which is commonly displayed by the pyroxenes of slowly cooled plutonic rocks, is only weakly and partially developed in some of the pyroxenes in this dyke.

Numerous physico-chemical parameters affect the character of pyroxenes. The most obvious ones are the pressure and temperature of crystallization, the rate of cooling and the liquid composition (see Dowty, 1980; Lofgren, 1980; Prewitt, 1980). The evolution of the various pyroxene assemblages of the MD dykes has been discussed by Hall *et al.* (1985). The temperatures of crystallization of such assemblages are best estimated from the graphical pyroxene thermometer of Lindsley (1983) and this does not suggest any abnormally high or low crystallization temperatures for these dykes. There is no evidence from the pyroxene chemistry to suggest that the crystallization pressures were in

any way anomalous (Gasparik, 1984) and the textures clearly indicate that the cooling rate could not have been sufficiently fast to effect unusual partitioning of the principal components Ca, Mg, and Fe (cf. Gamble and Taylor, 1980; Lofgren, 1980). The chemical composition and subsequent evolution of discrete liquid cells trapped between abundant large plagioclase primocrysts were probably the dominant factors in controlling the nature of the precipitating pyroxenes in GGU 120432. In particular, low oxygen fugacity (f_{O_2}) and differential ionic diffusion rates effected by variation in the activities of SiO_2, CaO, and FeO combined with local supercooling could all have played important roles. For example, a low f_{O_2} (and thus a potentially low Fe_2O_3 : FeO ratio) would have suppressed the precipitation of magnetite in favour of that of progressively Fe-rich pyroxene (Osborn, 1959; Grove *et al.*, 1982). This is mirrored petrogenetically by the development of the Fe-enrichment trend typical of evolving basic tholeiitic magma series (Irvine and Baragar, 1971). On the other hand, calc-alkaline lavas which generally crystallize under higher f_{O_2} conditions, commonly contain Fe–Ti oxide as an early phase in association with compositionally uniform, magnesian pyroxenes (Mueller, 1969; Fodor, 1971; Garcia, 1978; Grove *et al.*, 1982). Thus, it is perhaps significant that the Fe_2O_3 : FeO ratio of sample GGU 120432 is low (*c.*0.09). Similarly, a low f_{O_2} coupled with low a_{SiO_2} could have suppressed orthopyroxene crystallization in favour of the nucleation of more Fe-rich olivine (Campbell and Nolan, 1974). The typical sequence of tholeiite crystallization, in which a_{CaO} is effectively balanced by the almost simultaneous precipitation of calcic plagioclase and magnesian clinopyroxene in a relatively low f_{O_2} environment, usually leads to the simple progressive Fe-enrichment of subsequent pyroxenes (Carmichael, 1967; Wager and Brown, 1968). However, variation in the rate of plagioclase precipitation or perhaps its virtual cessation during supercooling (Gibb, 1974) could clearly effect a significant change in a_{CaO} and consequently the nature of local pyroxene precipitation.

Different complex pyroxene relationships occur in other generations of the MD dyke swarm (Hall *et al.*, 1985). For example, zoning from orthopyroxene or pigeonite cores through epitaxially overgrown subcalcic augite to ferroaugite margins is present in some of the MD3 dyke pyroxenes. In several cases this zoning is clear and can be simply explained by rising a_{CaO} (with rising a_{FeO}) after the retardation of the growth of large plagioclase primocrysts during the early stages of pyroxene crystallization, although the thermometric data are at variance with the apparently clear petrographic relationships, suggesting that such zoning from pigeonite to subcalcic augite is an up-temperature sequence (cf. fig. 9 inset). In the MD3 dyke sample GGU 155686, which is considerably more evolved (ionic Mg/(Mg + Fe) = 0.38) than the previously described MD2 sample 120432 (fig. 1, Table I), although BSE imagery confirms the presence of similar partially

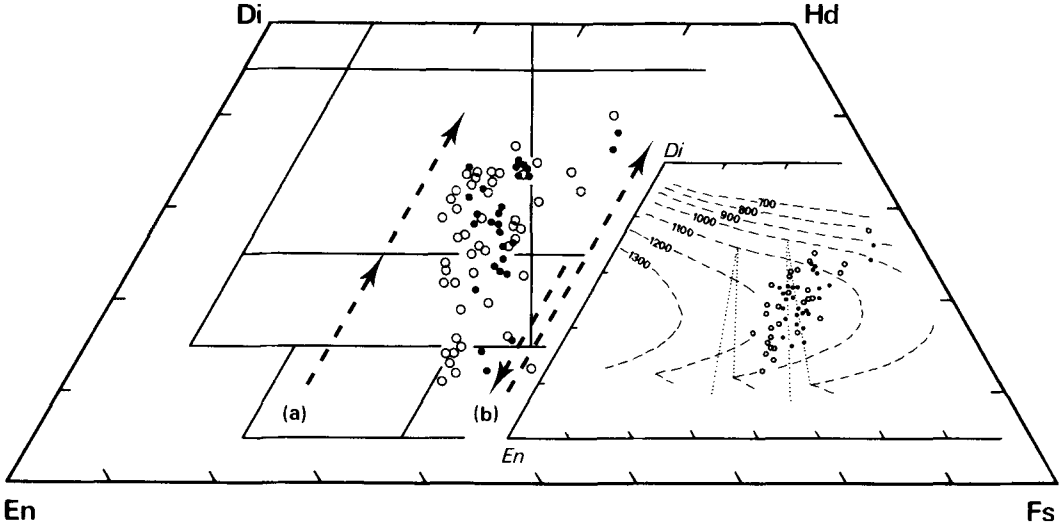

FIG. 9. Pyroxene compositions of two grains (16, filled circles; 22, open circles) in MD3 dyke sample GGU 155686 and possible crystallization sequences inferred from (*a*) core to margin zoning and (*b*) textural relationships identified by BSE imagery and inferred from thermometric data (inset).

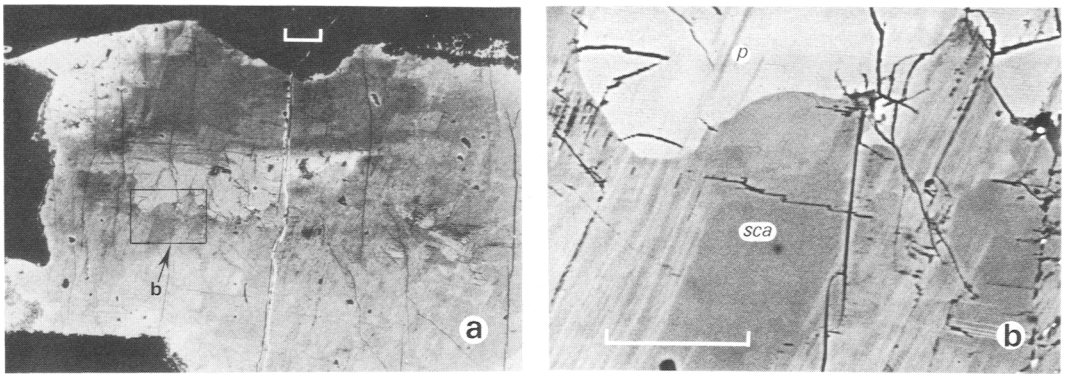

FIG. 10. (*a*) BSE image of grain 16 in MD3 dyke sample GGU 155686. Scale bar = 100 μm. (*b*) BSE image detail of field indicated by box on image (*a*) showing sutured contact between pigeonite (*p*) and sub-calcic augite (*sca*). Scale bar = 50 μm.

concentric, increasingly Ca-rich pyroxene zoning (figs. 9; 10*a*), the contacts between the core pigeonite and surrounding subcalcic augite are sharp and sutured (fig. 10*b*) and thus the growth sequence between these phases is not clear. These sutured contacts may indicate that early formed pigeonite was partially resorbed prior to or during the precipitation of subcalcic augite (fig. 9*a*), although this would again be at variance with the thermometric data. The less likely crystallization sequence subcalcic augite–pigeonite–ferroaugite (fig. 9*b*) is another possibility which, while it would agree with the thermometric data (fig. 9 inset), would also require a relatively complex evolution of a_{CaO} and a_{FeO}.

The only other rocks which have been reported so far with similar wide-ranging pyroxene assemblages are some lunar basalts, and there is a marked similarity between the schematic development of the MD2 pyroxenes (fig. 7) and the zoning of some lunar pyroxenes (Bence *et al.*, 1971; Boyd and Smith, 1971; Klein *et al.*, 1971; Kushiro *et al.*, 1971). The chemical changes which produced the variable pyroxene precipitation in lunar basalts were probably enhanced by extremely low f_{O_2} conditions (Haggerty, 1978; Papike, 1980), rapid cooling and turbulence during crystallization in the very low viscosity lunar magmas (Murase and McBirney, 1970; Boyd, 1971). There is little evidence for emplacement turbulence during the intrusion of the MD dykes (Williams, 1976) and none was found within the homogeneous dykes sampled for this study. It seems more likely that complex sequences of pyroxene precipitation in the case of hypabyssal terrestrial rocks are due to the internal differentiation of liquid cells trapped within a framework of earlier formed, growing plagioclase feldspars (cf. Nwe, 1975). The compositional complexity of the pyroxenes within each cell and from one cell to another is probably due both to differences in composition of the trapped liquid in each cell and to variable nucleation behaviour and ionic diffusion gradients across the cells as they cooled (Gibb, 1974; Dowty, 1980; Lofgren, 1980). Assemblages of such complex, sequentially crystallized pyroxenes are possibly restricted to, and appear to be fairly common (Hall and Hughes, unpublished data) in hypabyssal, low f_{O_2} tholeiitic rocks in which the cooling rate was sufficiently slow to prevent the quench growth of the isolated metastable grains often found in lavas, but was not slow enough to accommodate the complete equilibration of pyroxenes typical of plutonic rocks.

Acknowledgements. We would like to thank J. V. P. Long, A. Buckley, P. Treloar, and N. Charnley for making available and assisting with the electron microprobe facilities at the Departments of Earth Sciences at Cambridge and Oxford Universities. S. Moss, P. Bond, and A. Kearsley are thanked for their assistance with the scanning electron microscope facilities at Portsmouth and Oxford Polytechnics. We acknowledge the helpful comments of two anonymous reviewers. This paper is published with the permission of the Director of the Geological Survey of Greenland.

REFERENCES

Allaart, J. H. (1976) In *Geology of Greenland* (A. Escher and W. S. Watt, eds.). GGU, Copenhagen, pp. 121–51.

Arndt, N. T., and Fleet, M. E. (1979) *Am. Mineral.* **64,** 856–64.

Bence, A. E., Papike, J. J., and Lindsley, D. H. (1971) In *Proceedings of the second lunar science conference, vol. 1* (A. A. Levinson, ed.). MIT Press, Cambridge, pp. 559–74.

Boyd, F. R. (1971) *Carnegie Inst. Wash. Yearb.* **69,** 216–30.
——and Smith, D. (1971) *J. Petrol.* **12,** 439–65.
Brown, G. C., Hughes, D. J., and Esson, J. (1973) *Chem. Geol.* **11,** 223–9.
Campbell, I. H., and Nolan, J. (1974) *Contrib. Mineral. Petrol.* **48,** 205–19.
Carmichael, I. S. E. (1967) *Am. Mineral.* **52,** 1815–41.
Chadwick, B. (1969) *Tectonophys.* **8,** 247–64.
——and Coe, K. (1983) (compilers) *1 : 100 000 scale geological map, Buksefjorden, 63V1 Nord.* Geol. Surv. Greenland.
Dawes, P. R. (1970) *Rapp. Grønlands geol. Unders.* **29,** 60 pp.
Dowty, E. (1980) In *Physics of magmatic processes* (R. B. Hargraves, ed.). Princeton Univ. Press, Princeton, pp. 419–85.
Evensen, N. M., Hamilton, P. J., and O'Nions, R. K. (1978) *Geochim. Cosmochim. Acta,* **42,** 1199–212.
Ewart, A. (1976) *Contrib. Mineral. Petrol.* **58,** 1–22.
Fodor, R. V. (1971) *Earth Planet. Sci. Lett.* **11,** 385–90.
Gamble, R. P., and Taylor, L. A. (1980) Ibid. **47,** 21–33.
Garcia, M. O. (1978) *Earth Sci. Rev.* **14,** 147–65.
Gasparik, T. (1984) *Contrib. Mineral. Petrol.* **87,** 87–97.
Gibb, F. G. F. (1974) *Mineralg. Mag.* **39,** 641–53.
Grove, T. L., Gerlach, D. C., and Sando, T. W. (1982) *Contrib. Mineral. Petrol.* **80,** 160–82.
Haggerty, S. E. (1978) *Geophys. Res. Lett.* **5,** 443–6.
Hall, R. P., Hughes, D. J., and Friend, C. R. L. (1985) *J. Petrol.* **26,** 253–82.
Huebner, J. S., and Turnock, A. C. (1980) *Am. Mineral.* **65,** 225–71.
Irvine, T. N., and Baragar, W. R. A. (1971) *Can. J. Earth Sci.* **8,** 523–48.
Kalsbeek, F., and Taylor, P. N. (1985) *Contrib. Mineral. Petrol.* **89,** 307–16.
Klein, C., Jnr., Drake, J. C., and Frondel, C. (1971) In *Proceedings of the second lunar science conference, vol. 1* (A. A. Levinson, ed.). MIT Press, Cambridge, pp. 265–84.
Kushiro, I., Nakamura, Y., Kitayama, K., and Akimoto, S-I. (1971) Ibid. pp. 481–96.
Lindsley, D. H. (1983) *Am. Mineral.* **68,** 477–93.
Lofgren, G. (1980) In *Physics of magmatic processes* (R. B. Hargraves, ed.). Princeton Univ. Press, pp. 487–551.
Mori, T. (1978) *J. Petrol.* **19,** 45–65.
Mueller, R. F. (1969) *Hydration, oxidation, and the origin of the calc-alkali series.* NASA Springfield, 27 pp.
Murase, T., and McBirney, A. F. (1970) *Science,* **167,** 1491–3.
Myers, J. S. (1980) (compiler) *1 : 100 000 scale geological map, Sinarssuk, 63V2 Syd.* Geol. Surv. Greenland.
——(1982) (compiler) *1 : 100 000 scale geological map, Graedefjord, 63V1 Syd.* Geol. Surv. Greenland.
Nwe, Y. Y. (1975) *Contrib. Mineral. Petrol.* **49,** 285–300.
——(1976) Ibid. **55,** 105–26.
Osborn, E. F. (1959) *Am. J. Sci.* **257,** 609–47.
Papike, J. J. (1980) In *Reviews in mineralogy, vol. 7, Pyroxenes* (C. T. Prewitt, ed.). Mineral. Soc. Am., Washington, pp. 495–525.
Poldervaart, A., and Hess, H. H. (1951) *J. Geol.* **59,** 472–89.
Prewitt, C. T. (1980) (ed.) *Reviews in mineralogy, vol. 7, Pyroxenes.* Mineral. Soc. Am., Washington, 525 pp.
Rivalenti, G. (1975) *Can. J. Earth Sci.* **12,** 721–30.
Wager, L. R., and Brown, G. M. (1968) *Layered igneous rocks.* Oliver and Boyd, London, 588 pp.
Williams, H. R. (1976) *Geol. Mag.* **113,** 77–82.
Wilson, A. D. (1955) *Bull. geol. Surv. G.B.* **9,** 55–8.

[*Manuscript received 21 May 1985; revised 17 January 1986*]